Imaging cell size and permeability in biological tissue using the diffusion-time dependence of the apparent diffusion coefficient

Olaf Dietrich[1,2], Alexander Hubert[2] and Sabine Heiland[2]

[1] Josef Lissner Laboratory for Biomedical Imaging, Institute for Clinical Radiology, Ludwig-Maximilians-University Hospital Munich, Marchioninistr. 15, 81377 Munich, Germany

[2] Department of Neuroradiology, Heidelberg University Hospital, Im Neuenheimer Feld 400, 69120 Heidelberg, Germany

E-mail: od@dtrx.net

ELECTRONIC PREPRINT VERSION:

Not for commercial sale or for any systematic external distribution by a third party

Final version: *Phys Med Biol* 2014; **59**(12): 3081–3096

⟨URL: http://dx.doi.org/10.1088/0031-9155/59/12/3081⟩

Abstract. The purpose of this study was to analyze and evaluate a model of restricted water diffusion between equidistant permeable membranes for cell-size and permeability measurements in biological tissue. Based on the known probability distribution of diffusion distances after the diffusion time τ in a system of permeable membranes characterized by 3 parameters (membrane permeability P, membrane distance L, and free diffusivity D_0), an equivalent dimensionless model was derived with a probability distribution characterized by only a single (dimensionless) tissue parameter $\tilde{P}$. Evaluating this proposed model function, the dimensionless diffusion coefficient $\tilde{D}_{\mathrm{eff}}(\tilde{\tau};\,\tilde{P})$ was numerically calculated for 60 values of the dimensionless diffusion time $\tilde{\tau}$ and 35 values of $\tilde{P}$. Diffusion coefficients were measured in a carrot by diffusion-weighted magnetic resonance imaging (MRI) at 18 diffusion times between 9.9 and 1022.7 ms and fitted to the simulation results $\tilde{D}_{\mathrm{eff}}(\tilde{\tau};\,\tilde{P})$ to determine L, P, and D_0. The measured diffusivities followed the simulated dependence of $\tilde{D}_{\mathrm{eff}}(\tilde{\tau};\tilde{P})$. Determined cell sizes varied from 21 to 76 µm, permeabilities from 0.007 to 0.039 $\mu\mathrm{m}^{-1}$, and the free diffusivities from 1354 to 1713 $\mu\mathrm{m}^2/\mathrm{s}$. In conclusion, the proposed dimensionless tissue model can be used to determine tissue parameters (D_0, L, P) based on diffusion MRI with multiple diffusion times. Measurements in a carrot showed a good agreement of the cell diameter, L, determined by diffusion MRI and by light microscopy.

Key words: Diffusion-weighted magnetic resonance imaging; Biophysical mechanisms of MR diffusion; Restricted diffusion; Cell size; Permeable membranes

Introduction

In diffusion-weighted MRI (DWI), the random motion of molecules during a diffusion time τ causes a signal attenuation from which the apparent diffusion coefficient (ADC) can be calculated (Hahn 1950, Stejskal & Tanner 1965, Taylor & Bushell 1985, Le Bihan et al. 1986, Xu et al. 2007, Russell et al. 2012). For unrestricted diffusion (e. g., in pure liquids), the probability distribution of displacements, Δx, of molecules can be described by a Gaussian function and the average diffusion distance $\left(\overline{(\Delta x)^2}\right)^{1/2}$ of a particle is given by the standard deviation of the Gaussian distribution and is proportional to the square root of τ. If diffusion is restricted, e. g., by cell membranes in biological tissue, the mean displacement is smaller than in the case of free diffusion and the calculated ADC will decrease with increasing diffusion time in a characteristic way depending on the confining geometry (Woessner 1963, Stejskal 1965, Tanner & Stejskal 1968, Sen 2004, Grebenkov 2007). This dependence can be used to determine the pore size in porous media or the cell size in biological tissue by acquiring a series of diffusion-weighted images with different diffusion times and fitting the data to a model of restricted diffusion (Wayne & Cotts 1966, Tanner 1978, Zhong & Gore 1991, Knauss et al. 1999, Weber et al. 2009).

The purpose of the present study was to analyze and apply a model of restricted diffusion in a one-dimensional system of equidistant permeable membranes originally proposed by Powles et al. (1992) for cell size and permeability measurements in biological tissue.

Theory

Diffusion coefficient and displacement distribution

Molecular self diffusion in one dimension in a (macroscopically) homogeneous tissue can be described by a probability distribution $p(\Delta x, \tau;\, D_0, \mathcal{P})$ for a certain molecular displacement Δx at the end of a diffusion time interval τ. The probability distribution depends on the diffusion coefficient D_0 and may also depend (in particular in the case of non-Gaussian diffusion) on other parameters $\mathcal{P}$. In the simple case of one-dimensional Gaussian diffusion, the distribution is completely characterized by its variance, $\sigma^2 = 2D_0\tau$.

Diffusion between permeable barriers

In an infinite one-dimensional array of equidistant permeable barriers, the probability distribution p depends not only on the displacement, Δx, but on the initial and final positions, x_0 and $x = x_0 + \Delta x$, because of the microscopically inhomogeneous, periodic structure. The probability distribution p of the diffusion from x_0 to x in such an array

is (from Powles et al. (1992, App. B)):‡

$$\begin{aligned}\sqrt{4\pi D_0\tau}\, p(x,\tau;\, x_0;\, D_0, L, P) \;&=\; (1-f)^{|z|}\exp\big(-(|x-x_0|)^2/4D_0\tau\big)\\
&+\sum_{\substack{l=|z|\\ \text{step }2}}^{\infty}(1-f)^l f\,\left(\exp\left(\frac{-\big((l+1-z)L+x+x_0\big)^2}{4D_0\tau}\right)+\exp\left(\frac{-\big((l+1+z)L-x-x_0\big)^2}{4D_0\tau}\right)\right)\\
&+\sum_{\substack{l=|z|\\ \text{step }2}}^{\infty}\sum_{k=2}^{\infty}(1-f)^l f^k\prod_{j=2}^{k}\left(\frac{2j-1-(2z-1)(-1)^j+2l}{2j-1+(-1)^j}\right)\exp\left(\frac{-\big((l+k+(-1)^k z)L-(-1)^k x+x_0\big)^2}{4D_0\tau}\right)\\
&+\sum_{\substack{l=|z|\\ \text{step }2}}^{\infty}\sum_{k=2}^{\infty}(1-f)^l f^k\prod_{j=2}^{k}\left(\frac{2j-1+(2z+1)(-1)^j+2l}{2j-1+(-1)^j}\right)\exp\left(\frac{-\big((l+k-(-1)^k z)L+(-1)^k x-x_0\big)^2}{4D_0\tau}\right)\end{aligned}\tag{1}$$

with barrier distance L (barriers are positioned at $x_\mathrm{B} = \ldots, -\frac{3}{2}L, -\frac{1}{2}L, \frac{1}{2}L, \frac{3}{2}L, \ldots$), permeability P (unit: m^{-1})§, and free diffusivity (between barriers) D_0; x_0 is located in the central layer, i. e., $-\frac{1}{2}L \le x_0 \le \frac{1}{2}L$, and z describes the 'slice number' of the final position x, i. e., $(z-\frac{1}{2})L < x < (z+\frac{1}{2})L$, i. e., $|z|$ is also the number of membranes between the initial and final position. k and l give the number of reflections and transmissions, respectively, for a certain trajectory between x_0 and x. $f = f(\mathcal{X};\tau,P,D_0)$ is the reflection coefficient (and $(1-f)$ the transmission coefficient) with

$$f(\mathcal{X};\tau,P,D_0) = 1 - 2P\int_0^\infty \mathrm{d}s\,\exp\left(-\left(2Ps+\frac{s^2}{4D_0\tau}+\frac{s}{2D_0\tau}\mathcal{X}\right)\right),\tag{2}$$

where $\mathcal{X}$ is to be replaced by the spatial argument of the exponential function that multiplies f; e. g., $\mathcal{X} = (l+1+z)L - x - x_0$ for the second addend of the second line of (1). This probability distribution can be used to calculate an effective diffusion-time-dependent diffusion coefficient $D_\mathrm{eff}(\tau; D_0, L, P)$.

For long diffusion times $\tau \gg L^2/D_0$, a limiting effective diffusion coefficient D_∞ exists with (Powles et al. 1992)

$$D_\infty = D_0/(1+(PL)^{-1}).\tag{3}$$

For very short diffusion times and impermeable membranes, the initial, approximately linear behavior of $D_\mathrm{eff}(\tau)/D_0 - 1$ with respect to $\sqrt{\tau}$ is given by Mitra et al. (1992) as $-4/(3\sqrt{\pi})(S/V)\sqrt{D_o\tau}$ in the case of one-dimensional diffusion. The surface-to-volume ratio S/V of a system of parallel barriers is $S/V = \lim_{x\to\infty} 2x^2/(Lx^2) = 2/L$, yielding

$$\frac{D_\mathrm{eff}(\tau)}{D_0} - 1 = \frac{-8}{3\sqrt{\pi}L}\sqrt{D_o\tau} + O(\sqrt{\tau}^2).\tag{4}$$

‡ The lower summation limit in the second line was corrected from 0 to $|z|$ with a step size of 2, since a minimum of $|z|$ transmissions is always required for a trajectory from x_0 to x.

§ We follow Powles et al. by defining the permeability in units of m^{-1}; a frequently found alternative is to describe permeabilities by $P' = P\cdot D_0$, i. e., in units of m/s.

Dimensionless units

To simplify the analysis and numerical handling of (1) by reducing the number of physical parameters, we now introduce dimensionless quantities proportional to x, τ, and P by defining $\tilde{x} = x/L$, $\tilde{x}_0 = x_0/L$, $\tilde{\tau} = 2D_0\tau/L^2$ (i. e., $\tilde{\tau}$ is the variance $E\big((\Delta\tilde{x})^2\big)$ of the unrestricted dimensionless diffusion distribution), and $\tilde{P} = LP$. The diffusion coefficient $\tilde{D}_0$ is then simply $\tilde{D}_0 = \frac{1}{2\tilde{\tau}}E\big((\Delta\tilde{x})^2\big) = \frac{1}{2}$, other diffusion coefficients are scaled to $\tilde{D} = D/(2D_0)$, and b-values (diffusion weightings) accordingly to $\tilde{b} = 2D_0 b$. The effective long-time diffusion coefficient from (2) is then

$$\tilde{D}_\infty = \frac{1}{2}/(1 + 1/\tilde{P}) \tag{5}$$

and the initial behavior of $\tilde{D}_{\rm eff}(\tilde{\tau})$ can be calculated from (4) by substituting $\tau = L^2\tilde{\tau}/(2D_0)$ and $D_{\rm eff} = 2D_0\tilde{D}_{\rm eff}$:

$$\tilde{D}_{\rm eff}(\tilde{\tau}) - \frac{1}{2} = \frac{-4}{3\sqrt{2\pi}}\sqrt{\tilde{\tau}} + O(\sqrt{\tilde{\tau}}^2) = \frac{-2}{3}\sqrt{\frac{2}{\pi}}\sqrt{\tilde{\tau}} + O(\sqrt{\tilde{\tau}}^2). \tag{6}$$

The original probability density p (having the units of an inverse length) is replaced by the dimensionless density $\tilde{p} = Lp$ (with normalization $\int_{-\infty}^{\infty}\tilde{p}(\tilde{x})\mathrm{d}\tilde{x} = 1$), which does not depend anymore on L (since $\tilde{L} = 1$) or on D_0; thus, the only remaining parameter required to describe the probability distribution $\tilde{p}$ is the dimensionless permeability $\tilde{P}$:

$$\begin{aligned}
\sqrt{2\pi\tilde{\tau}}\,\tilde{p}(\tilde{x},\tilde{\tau};\,\tilde{x}_0;\,\tilde{P}) \;=\;& (1-f)^{|z|}\exp\big(-(|\tilde{x}-\tilde{x}_0|)^2/2\tilde{\tau}\big) \\
&+ \sum_{\substack{l=|z|\\ \text{step }2}}^{\infty}(1-f)^l f\left(\exp\left(\frac{-\big((l+1-z)+\tilde{x}+\tilde{x}_0\big)^2}{2\tilde{\tau}}\right)+\exp\left(\frac{-\big((l+1+z)-\tilde{x}-\tilde{x}_0\big)^2}{2\tilde{\tau}}\right)\right) \\
&+ \sum_{\substack{l=|z|\\ \text{step }2}}^{\infty}\sum_{k=2}^{\infty}(1-f)^l f^k\prod_{j=2}^{k}\left(\frac{2j-1-(2z-1)(-1)^j+2l}{2j-1+(-1)^j}\right)\exp\left(\frac{-\big((l+k+(-1)^k z)-(-1)^k\tilde{x}+\tilde{x}_0\big)^2}{2\tilde{\tau}}\right) \\
&+ \sum_{\substack{l=|z|\\ \text{step }2}}^{\infty}\sum_{k=2}^{\infty}(1-f)^l f^k\prod_{j=2}^{k}\left(\frac{2j-1+(2z+1)(-1)^j+2l}{2j-1+(-1)^j}\right)\exp\left(\frac{-\big((l+k-(-1)^k z)+(-1)^k\tilde{x}-\tilde{x}_0\big)^2}{2\tilde{\tau}}\right)
\end{aligned} \tag{7}$$

The reflection coefficient $f = f(\tilde{\mathcal{X}};\tilde{\tau},\tilde{P})$ is then calculated according to (2) after substituting $\tilde{s} = s/L$ for s as

$$f(\tilde{\mathcal{X}};\tilde{\tau},\tilde{P}) = 1 - 2\tilde{P}\int_0^\infty \mathrm{d}\tilde{s}\,\exp\left(-\left(2\tilde{P}\tilde{s} + \frac{\tilde{s}^2}{2\tilde{\tau}} + \frac{\tilde{s}}{\tilde{\tau}}\tilde{\mathcal{X}}\right)\right), \tag{8}$$

where $\tilde{\mathcal{X}}$ is again to be replaced by the dimensionless ("spatial") argument of the exponential function that multiplies f. This integral can be solved using the error

function $\mathrm{erf}(x)$ as well as the complementary error function $\mathrm{erfc}(x) = 1 - \mathrm{erf}(x)$ and is¶

$$\begin{aligned} f(\tilde{\mathcal{X}};\, \tilde{\tau}, \tilde{P}) &= 1 - 2\tilde{P} \int_0^\infty \mathrm{d}\tilde{s}\, \exp\left(-\left(\left(2\tilde{P} + \frac{\tilde{\mathcal{X}}}{\tilde{\tau}}\right)\tilde{s} + \frac{1}{2\tilde{\tau}}\tilde{s}^2 \right) \right) \\ &= 1 - 2\tilde{P}\left[\sqrt{\frac{\pi}{2}}\sqrt{\tilde{\tau}}\, \exp\left(\frac{\tilde{\tau}}{2}\left(2\tilde{P} + \frac{\tilde{\mathcal{X}}}{\tilde{\tau}}\right)^2 \right) \mathrm{erf}\left(\frac{\tilde{s}}{\sqrt{2\tilde{\tau}}} + \sqrt{\frac{\tilde{\tau}}{2}}\left(2\tilde{P} + \frac{\tilde{\mathcal{X}}}{\tilde{\tau}}\right) \right) \right]_0^\infty \\ &= 1 - 2\tilde{P}\sqrt{\frac{\pi}{2}}\sqrt{\tilde{\tau}}\, \exp\left(\frac{\tilde{\tau}}{2}\left(2\tilde{P} + \frac{\tilde{\mathcal{X}}}{\tilde{\tau}}\right)^2 \right) \mathrm{erfc}\left(\sqrt{\frac{\tilde{\tau}}{2}}\left(2\tilde{P} + \frac{\tilde{\mathcal{X}}}{\tilde{\tau}}\right) \right). \end{aligned} \tag{9}$$

Unfortunately, the product $\exp(x^2)\mathrm{erfc}(x)$ is difficult to evaluate numerically since the first factor goes to infinity rather quickly and the second one to zero. It can, however, be approximated, e. g., as $\left[\frac{1}{2}\sqrt{\pi}\left(x + \sqrt{2[1-(1-2/\pi)\exp(-x\sqrt{5/7})] + x^2}\right)\right]^{-1}$ (with a relative error lower than 10^{-6} for $x > 23$) according to a result by Spanier & Oldham given by Lether (1990, Eq. 2); see also (Kim et al. 1990).

Integrating $\tilde{p}$ over all initial positions $-\frac{1}{2} < \tilde{x}_0 < \frac{1}{2}$ gives the averaged probability density $\bar{p}$ for a displacement $\Delta\tilde{x} = \tilde{x} - \tilde{x}_0$:

$$\bar{p}(\Delta\tilde{x};\, \tilde{\tau}, \tilde{P}) = \int_{-1/2}^{1/2} \mathrm{d}\tilde{x}_0\, \tilde{p}(\Delta\tilde{x} + \tilde{x}_0, \tilde{\tau};\, \tilde{x}_0;\, \tilde{P}). \tag{10}$$

In dimensionless units, the attenuation of the signal intensity $S(\tilde{\tau}, \tilde{b};\, \tilde{P})/S_0$ can be calculated from $\bar{p}$ as before by another spatial integration based on the dimensionless diffusion weighting $\tilde{b}$ or, approximately, assuming the short-gradient approximation, using the variance of the distribution $\bar{p}$:

$$S(\tilde{\tau}, \tilde{b};\, \tilde{P})/S_0 = \int_{-\infty}^{\infty} \bar{p}(\Delta\tilde{x}, \tilde{\tau};\, \tilde{P}) \exp\left(\mathrm{i}\sqrt{\frac{\tilde{b}}{\tilde{\tau}}}\, \Delta\tilde{x} \right) \mathrm{d}\Delta\tilde{x} \tag{11}$$

$$\approx 1 - \frac{\tilde{b}}{2\tilde{\tau}} E\big((\Delta\tilde{x})^2\big), \tag{12}$$

and the (dimensionless) diffusion coefficient $\tilde{D}_{\mathrm{eff}} = D_{\mathrm{eff}}/(2D_0)$ (ranging from 0 to $\frac{1}{2}$) is

$$\tilde{D}_{\mathrm{eff}}(\tilde{\tau}, \tilde{b};\, \tilde{P}) = -\frac{\ln(S(\tilde{\tau}, \tilde{b};\, \tilde{P})/S_0)}{\tilde{b}} \approx \frac{1}{2\tilde{\tau}} E\big((\Delta\tilde{x})^2\big). \tag{13}$$

This result can be used to calculate $\tilde{D}_{\mathrm{eff}}$ numerically for arbitrary diffusion times and permeabilities (as the only parameter related to structure) by simulating the probability distribution $\tilde{p}$.

Knowing the dependence of the dimensionless diffusion coefficient $\tilde{D}_{\mathrm{eff}}$ on $\tilde{\tau}$ and $\tilde{P}$, it becomes possible to scale and fit this family of curves to actually measured diffusion coefficients $D_{\mathrm{meas}}(\tau)$ with the aim to determine the tissue parameters D_0, L, and P. The model function $D_{\mathrm{eff}}(\tau; D_0, L, P)$ is obtained from $\tilde{D}_{\mathrm{eff}}$ by scaling of the function

¶ The integral of $\exp(-(ax + bx^2))$ is $\frac{\sqrt{\pi}}{2\sqrt{b}}\exp(\frac{a^2}{4b})\mathrm{erf}(\sqrt{b}x + \frac{a}{2\sqrt{b}})$.

itself as well as of the parameters τ and P according the definitions of the dimensionless quantities:

$$D_{\text{eff}}(\tau; D_0, L, P) = 2D_0 \cdot \tilde{D}_{\text{eff}}\Big(\frac{2D_0}{L^2} \cdot \tau;\ L \cdot P\Big). \tag{14}$$

Methods

Simulations

We evaluated (7) (using the aforementioned approximation for $\exp(x^2)\text{erfc}(x)$ if $x \geq 23$) for a large range of (dimensionless) diffusion times $\tilde{\tau}$ (60 values between 0.000 016 and 225, scaled such that $\sqrt[4]{\tilde{\tau}}$ is approximately linearly distributed) and permeabilities $\tilde{P}$ (35 values between 0 and 30, with approximately linear distribution of $\sqrt{\tilde{P}}$).

The symmetric probability distribution $\bar{p}(\Delta\tilde{x}, \tilde{\tau}, \tilde{P})$ in (10) was evaluated for 501 evenly spaced diffusion distances $\Delta\tilde{x}$ $(= \tilde{x} - \tilde{x}_0)$ between 0 and $\Delta\tilde{x}_{\text{max}}$ by averaging ('integrating') over 501 evenly spaced values of initial positions $\tilde{x}_0$ between $-\frac{1}{2}$ and $\frac{1}{2}$. The maximum considered diffusion distance $\Delta\tilde{x}_{\text{max}}$ was defined depending on the standard deviation $\sigma_0 = \sqrt{\tilde{\tau}}$ of the original Gaussian distribution and on the effective standard deviation $\sigma_\infty = \sqrt{\tilde{\tau}/(1 + 1/\tilde{P})} < \sigma_0$ of the Powles distribution as

$$\Delta\tilde{x}_{\text{max}} = \begin{cases} 9\,\sigma_\infty & \text{for } \sigma_\infty \geq 1.5 \quad (\text{“long-}\tau\text{” experiments}) \\ 13.5 & \text{for } \sigma_\infty < 1.5 \text{ and } \sigma_0 > 1.5 \\ 9\,\sigma_0 & \text{for } \sigma_0 \leq 1.5 \quad (\text{“short-}\tau\text{” experiments}). \end{cases} \tag{15}$$

Thus, extremely improbable, long diffusion distances are excluded in the case of long-τ experiments and membranes with (very) low permeability.

Then the effective diffusion coefficient $\tilde{D}_{\text{eff}}(\tilde{\tau}, \tilde{P})$ was calculated using the variance of the distribution $\bar{p}(\Delta\tilde{x}, \tilde{\tau}, \tilde{P})$ according to (13). The infinite sums in (7) were evaluated for a minimum of 10 and a maximum of 500 addends; sum evaluation was stopped if the relative increment became lower than twice the floating-point precision.

Simulations were performed with self-written C routines (parallelization with OpenMP (http://openmp.org)) on a standard desktop PC (Intel Core2 Quad Q9550, 2.83 GHz).

Measurements

Diffusion measurements were performed on a 2.35-Tesla scanner (Biospec 24/40, Bruker Medical, Ettlingen, Germany) with a maximum gradient strength of 200 mT/m and a minimum ramp time of 80 µs. A carrot was used as diffusion phantom with variable cell sizes. Measurements were performed at room temperature (20 °C).

A diffusion-weighting stimulated-echo single-shot echoplanar imaging pulse sequence with 9 different b-values (0, 50, 100, ..., 400 s/mm^2) was applied in 2 orthogonal in-plane diffusion directions: along readout (horizontally displayed) and along phase-encoding (vertically displayed) direction. 18 different diffusion times $\tau = \Delta - \frac{\delta}{3}$ between

9.9 ms and 1022.7 ms were evaluated (diffusion gradient duration $\delta = 4$ ms, interval between gradient onsets Δ between 11.25 and 1024 ms) with varying number of signal averages between 2 for short τ and 16 for the longest τ. Other imaging parameters were: $T_R = 3000$ ms, $T_E = 45$ ms, receiver bandwidth: 200 kHz, matrix size 128×64 interpolated to 128×128, reconstructed voxel dimensions $0.39 \times 0.39 \times 4\,\text{mm}^3$. The total scan time for all 9 diffusion weightings, 18 diffusion times, and 2 diffusion directions was about 110 minutes.

The cell sizes within 2 thin slices of 2 carrots of the same cultivar (variety) were also determined by conventional light microscopy in 6 different areas positioned radially from the center of the carrot to the periphery. Mean values and standard deviations of cell sizes in radial and azimuthal orientation were obtained by averaging the measured dimensions of several ($n > 6$) cells.

Data evaluation

From the measured diffusion-weighted data, ADC maps $D_{\text{meas}}(\tau; x, y)$ were calculated pixelwise for each diffusion time using the logarithm of the signal attenuation and a linear regression algorithm.

The diffusion coefficients $D_{\text{meas}}(\tau)$ were then used to estimate the tissue parameters (D_0, L, P) from the proposed dimensionless model (7) and from (14) with a non-linear Levenberg-Marquardt least-squares fit algorithm by minimizing the difference $\big(D_{\text{eff}}(\tau; D_0, L, P) - D_{\text{meas}}(\tau)\big)^2$. Since a direct numerical evaluation of (7), (10), and (13) in the non-linear fit routine is too computationally expensive for frequently repeated function calls, the fit routine was based on the pre-computed simulation results $\tilde{D}_{\text{eff}}(\tilde{\tau}, \tilde{P})$ on the 60×35 grid mentioned above. For this purpose, we determined $\tilde{\tau}$ and $\tilde{P}$ from τ, D_0, L, and P in each step of non-linear fitting; then, we used a two-dimensional linear interpolation between the simulated data points $\tilde{D}_{\text{eff}}(\tilde{\tau}, \tilde{P})$ on the grid to calculate $D_{\text{eff}}(\tau; D_0, L, P)$ as defined in (14).

Fitting was performed (a) on a pixel-by-pixel basis generating parameter maps and (b) for 4 sets of 6 regions of interest (ROIs) (region size: 16 pixels) at MR-morphologically different appearing spatial localizations (cf. figure 1). The ROIs were defined such that – assuming cylindrical symmetry of the carrot – always 4 regions (one from each ROI set) correspond to one ROI used for light microscopy; thus, 4 equivalent regions could be combined for statistical evaluation of MRI data, and mean values as well as standard deviations of all tissue parameters for 6 different ROI positions could be obtained: ROI sets I and II in data with horizontal diffusion-weighting together with ROI sets III and IV in data with vertical diffusion-weighting contain only data with radial ADCs. ROI sets I and II in data with vertical diffusion-weighting together with ROI sets III and IV in data with horizontal diffusion-weighting contain only data with azimuthal ADCs; see figure 1a,b. GNU Octave (`http://www.octave.org`) was used for all fitting (`leasqr` routine) and data interpolation.

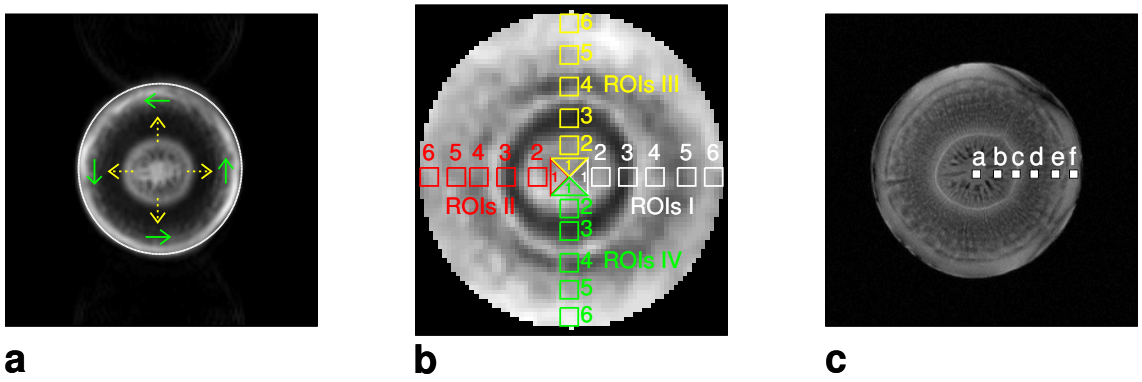

Figure 1. Regions of interest (ROIs) used for evaluation. (a) Example of a $b = 0$ image of diffusion-weighted data together with the circle (white) that defines the mask for pixelwise evaluation. The radial (dotted, yellow) and azimuthal (solid, green) in-plane orientations are indicated by arrows. (b) Masked ADC map with 4 sets (I, II, III, IV) of 6 ROIs $(1, \ldots, 6)$. Each ROI contains 16 pixels; 4×4 pixels in the square ROIs and a triangular quarter of $8 \times 8 = 64$ pixels in the central region. (c) Smaller regions at similar positions (a, ..., f) were used for light-microscopical cell size measurements.

Results

The results of the simulations are shown in figure 2a as a family of functions of $\sqrt{\tilde{\tau}}$. For short diffusion times, the effective diffusion coefficients goes to $\frac{1}{2} = \tilde{D}_0$ for all permeabilities, $\tilde{P}$. For very short diffusion times, the slope $\partial \tilde{D}_{\text{eff}}(\tilde{\tau})/\partial\sqrt{\tilde{\tau}}$ becomes approximately independent of the permeability, $\tilde{P}$ (figure 2b). The average initial slope (mean over all 35 curves) is approximately -0.531. For long diffusion times, the diffusion coefficient stays approximately constant at its limiting value $\tilde{D}_\infty$. The theoretical and simulated dependence of $\tilde{D}_\infty$ on the permeability $\tilde{P}$ is shown in figure 3; generally, the simulated values of $\tilde{D}_\infty$ agree well with the theory (5), but a small systematic deviation of up to 4 % is found for small permeabilities $\tilde{P} \approx 1$. The total computation time of the simulations was about 15:06 hours.

The acquired signals $S(b)$, from which the diffusion coefficients $D_{\text{meas}}(\tau)$ were calculated, exhibited a highly monoexponential behavior over the b-value range from 0 to 400 s/mm^2. The results $D_{\text{meas}}(\tau)$ of each evaluated ROI (mean value and standard deviation over 4 region sets (I, II, III, IV) with appropriate diffusion orientation) are shown in figure 4 as a function of the square root of the diffusion time. The resulting tissue parameters (calculated individually for all 24 ROIs and then averaged over 4 corresponding region sets) are shown in table 1; the cell size varies between 21 and almost 80 µm and the permeabilities lie between 0.007 and 0.039 µm^{-1}. The free diffusion coefficient D_0 varies between about 1350 and 1710 µm^2/s. The corresponding fit curves in figure 4 are based on the mean values of the tissue parameters (D_0, L, P) shown in table 1.

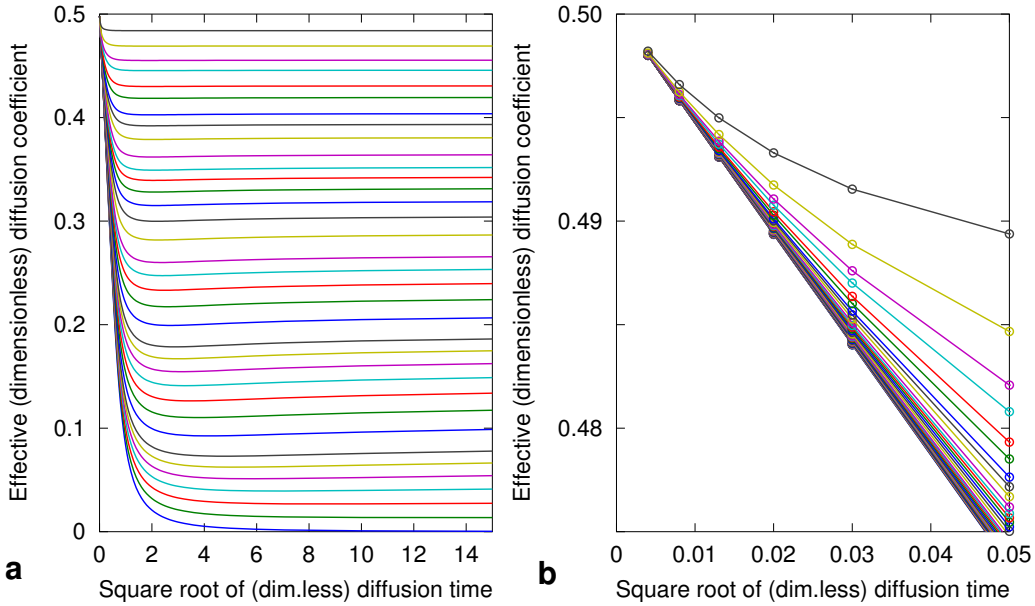

Figure 2. (a) Simulation results for permeabilities $\tilde{P}$ in the range from 0 (bottom curve) to 30.0 (top curve). (b) Magnified simulation results at very short scaled diffusion times $\tilde{\tau}$. Note that the limiting slope of all curves for $\tilde{\tau} \to 0$ is (approximately) independent of the permeability.

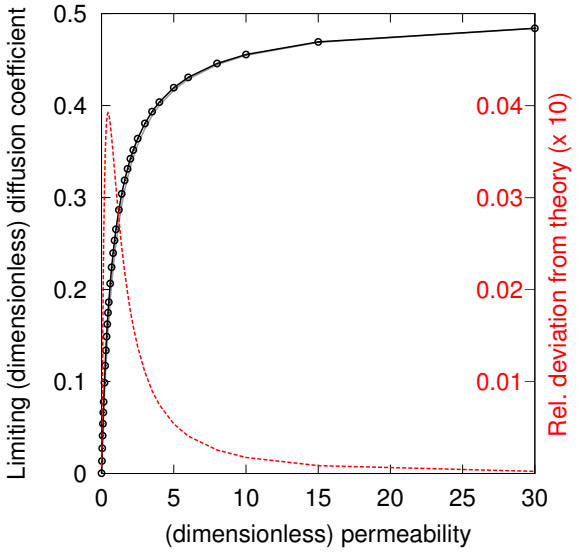

Figure 3. Dependence of $\tilde{D}_\infty$ on the permeability, $\tilde{P}$. The difference between simulations (black circles and line) and theoretical values (gray line) is plotted as dashed red line (normalized to $\tilde{D}_0$ and scaled up by a factor of 10).

Table 1. Tissue parameters from MRI and light-microscopy evaluation

Diffusion MRI				Light microscopy (diameter, µm)		
ROI	L (µm)	P (µm^{-1})	D_0 (µm^2/s)	ROI	carrot #1	carrot #2
Radial in-plane orientation:						
1	72.6 ± 3.0	0.007 ± 0.003	1713 ± 19	a	88.4 ± 26.5	86.7 ± 19.4
2	61.4 ± 3.8	0.009 ± 0.003	1658 ± 46	b	62.7 ± 19.5	66.3 ± 12.5
3	24.5 ± 1.4	0.016 ± 0.004	1422 ± 33	c	18.0 ± 4.4	24.3 ± 3.5
4	29.2 ± 4.3	0.027 ± 0.007	1531 ± 82	d	46.4 ± 11.5	51.8 ± 8.7
5	32.4 ± 5.8	0.026 ± 0.008	1568 ± 21	e	39.3 ± 4.1	44.2 ± 10.9
6	36.9 ± 4.3	0.030 ± 0.004	1625 ± 15	f	25.1 ± 8.2	22.9 ± 4.9
Azimuthal in-plane orientation:						
1	76.2 ± 4.7	0.007 ± 0.003	1711 ± 24	a	81.9 ± 9.8	76.9 ± 25.4
2	70.5 ± 4.1	0.009 ± 0.003	1661 ± 22	b	89.3 ± 18.0	66.8 ± 20.7
3	21.3 ± 1.1	0.013 ± 0.004	1354 ± 26	c	19.6 ± 3.3	22.4 ± 6.3
4	24.0 ± 3.9	0.028 ± 0.009	1514 ± 36	d	52.4 ± 10.9	53.5 ± 9.8
5	38.5 ± 11.0	0.031 ± 0.010	1592 ± 33	e	47.5 ± 10.9	56.7 ± 18.0
6	54.0 ± 8.8	0.039 ± 0.009	1656 ± 33	f	62.7 ± 17.5	58.5 ± 10.9

Results of the light-microscopy measurements of cell sizes are also presented in table 1 and agree well (both in trend and quantitatively) with the MRI data. The cell size determined by light microscopy is about 60…90 µm in the center (ROIs a and b), has a first minimum of about 20 µm (ROI c) at about one third of the radius, increases then again to about 40…50 µm (ROIs d and e), and reaches a second minimum (at least in radial direction) at the border with about 20 µm (ROI f). At this last position, the cell size is most anisotropic with a azimuthal diameter of about 60 µm.

Parameter maps of L, P, and D_0 obtained from pixelwise evaluation of diffusion-weighted MRI data are shown in figure 5a–f; the relative difference between these parameters determined from acquisitions with diffusion weighting in horizontal and vertical orientation is shown in figure 5g–i. This relative difference is substantially smaller for the free diffusion coefficient, D_0, than for the cell size and permeability. A positive difference of the cell size (i. e., a horizontally oriented cell shape) is observed at the top and bottom of the image and a negative one (i. e., a vertically oriented cell shape) at the left and right periphery; both results together indicate an azimuthally prolonged shape of the cell in the periphery. A similar pattern can be found at the center of the object, while at about one third of the radius the pattern is rotated by 90° (horizontal orientation at the left and right, vertical orientation at the bottom and top, which is compatible with radially oriented cell shapes in this circular region). The computation of each set of parameter maps took about 135 s (for about 3700 non-masked pixels).

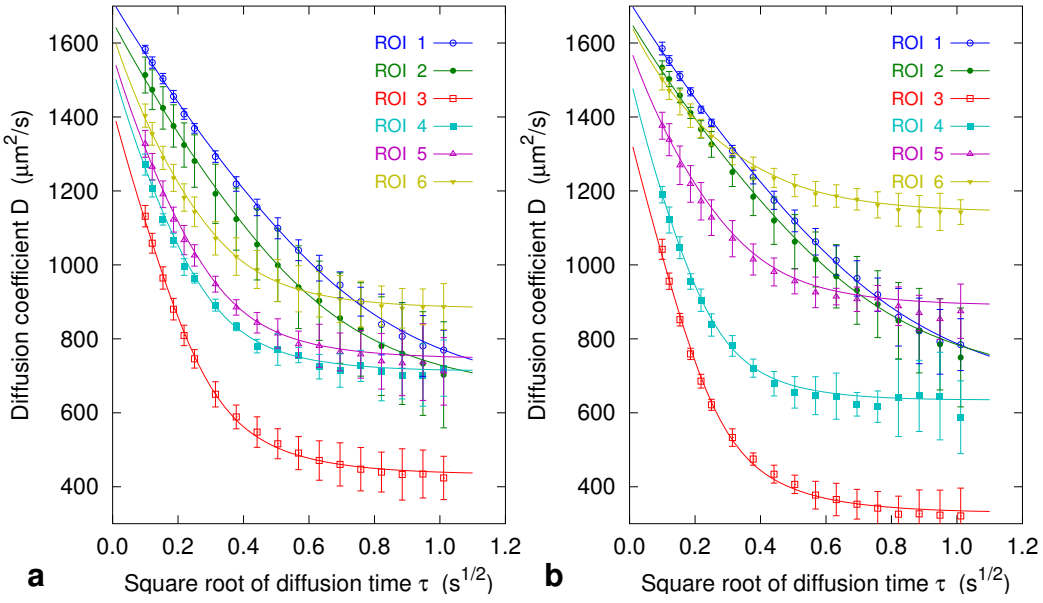

Figure 4. Evaluation of regions of interest; diffusion weighting in (a) radial and (b) azimuthal orientation. The measured diffusion coefficients are shown as colored circles (mean values over 4 region sets) with error bars (standard deviation over 4 region sets); the fitted model function as solid lines. (Regions: 1 – blue, 2 – dark green, 3 – red, 4 – cyan, 5 – magenta, 6 – light green.)

Discussion

The simulations result in a family of curves, $\tilde{D}_{\mathrm{eff}}(\tilde{\tau};\,\tilde{P})$ (figure 2), which show the expected behavior known from Powles et al. (1992) and, in similar form, from several other publications (Pfeuffer et al. 1998, Fieremans et al. 2010, Yablonskiy & Sukstanskii 2010, Kunz et al. 2013). In particular, the characteristic minimum of the diffusion coefficient observable at about $\sqrt{\tilde{\tau}} = 2$ for intermediate permeabilities is also present in the data shown by Powles et al. (1992); it is probably related to the substantial deviation of the statistical distribution of diffusion distances from a normal distribution in this parameter range. For long diffusion times, the simulated asymptotic effective diffusion coefficients (figure 3) agree reasonably well with the theory (5). The slightly increased values by at most about 4 % of the free diffusion coefficient, $\tilde{D}_0$, for low and intermediate permeabilities are independent of the chosen discretization parameters and appear also for even longer diffusion times than those assessed in our simulation; we did not find any numerical or physical explanation for this behavior. The initial slope $\partial\tilde{D}_{\mathrm{eff}}(\tilde{\tau})/\partial\sqrt{\tilde{\tau}}$ of -0.531 agrees well with the theoretical value of $-\frac{2}{3}\sqrt{\frac{2}{\pi}} = -0.531923\ldots$ (cf. (6)).

The curves for the chosen parameter range for $\tilde{P}$ cover almost uniformly the complete plane $(\tilde{\tau}, \tilde{D}_{\mathrm{eff}})$ in figure 2a. The maximum evaluated diffusion time, $\tilde{\tau}_{\max} = 225$, corresponds to a physical diffusion time of $\tau_{\max} \approx 3.8\,\mathrm{s}$ (calculated for a free diffusion coefficient $D_0 = 3000\,\mu\mathrm{m}^2/\mathrm{s}$ and a cell size of $L = 10\,\mu\mathrm{m}$); this diffusion time is somewhat

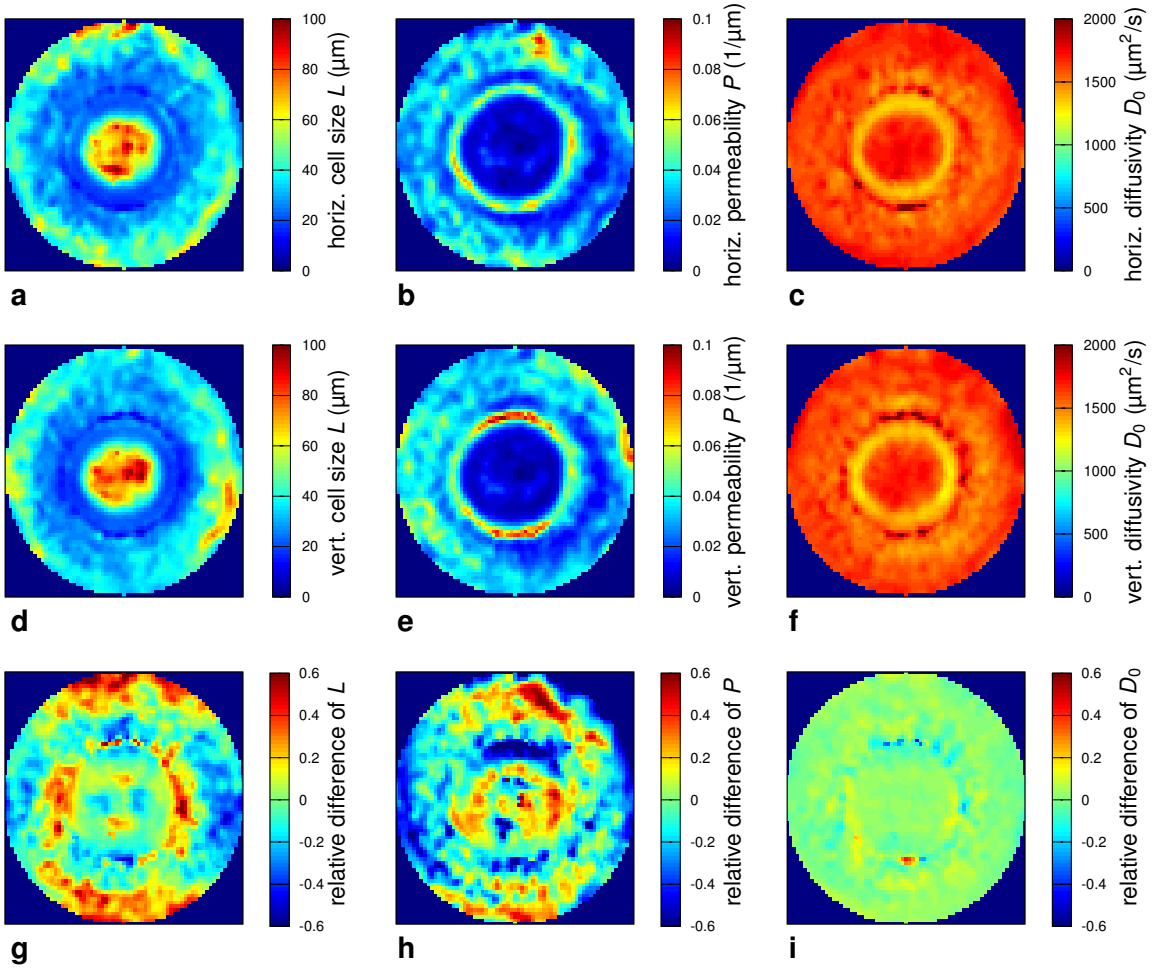

Figure 5. Parameter maps. Top row (a–c): parameters from acquisitions with diffusion weighting in horizontal orientation; central row (d–f): parameters from acquisitions with diffusion weighting in vertical orientation; bottom row (g–i): relative difference between horizontal and vertical orientation. Left column: cell size (µm); central column: permeability (μm^{-1}); right column: free diffusion ($\mu m^2/s$).

longer than the maximum diffusion times that can be assessed experimentally due to the T_1 signal decay during the stimulated-echo mixing time. Thus, the parameter ranges should be adequate to cover all experimental data.

The measurement results demonstrate a good quantitative agreement of cell diameters measured conventionally (by light microscopy) and by DWI with varying diffusion times; particularly, since no adjustable calibration parameters were used in our approach. The anisotropy of the cell diameters in the periphery (corresponding to an azimuthal orientation of cells) is clearly demonstrated by both methods; the higher anisotropy observed by microscopy is probably due to a more peripheral region (the border pixels of the carrot had to be removed from the DWI analysis due to low signal intensity). Remaining deviations can be explained by the inaccuracies of the light microscopy (including the differences between the samples and regions assessed

with both methods) and the fact that the mathematical model is a one-dimensional model based on parallel planes with constant distances while the cell shape is three-dimensional and irregular.

The measurement itself might be improved by further reducing the shortest diffusion time to values below 10 ms, thus enabling a better estimation of the initial slope of the measured curve $D_{\mathrm{meas}}(\sqrt{\tau})$ and the related parameters L and P. This, however, is hardly possible with conventional diffusion-gradient schemes and requires, for example, oscillating diffusion gradients (Van et al. 2014, Pyatigorskaya et al. 2013, Portnoy et al. 2013). Higher b-values than $400\,\mathrm{s/mm^2}$ were desirable to obtain a higher dynamic intensity range, but would further prolong the shortest possible diffusion time. In this study, we compensated for the lower dynamic range by increasing the number of b-values to 9, which enhances the precision of the calculated diffusion coefficients. The data evaluation might also be improved particularly for very short diffusion times by considering an additional correction term accounting for the increasingly inaccurate short-gradient approximation; cf. Grebenkov (2007, section VI. D)

The determined "free" diffusion coefficients, D_0, vary around $1600\,\mathrm{\mu m^2/s}$, which is about 20 % below the diffusion coefficient of pure water at room temperature. This may be explained by additional diffusion obstacles in a sub-cellular scale such as cell organelles or intracellular macromolecules. Compared with the cell size maps, the D_0 maps show only little spatial variation in good agreement with the assumption that D_0 is independent of the cell size.

The results for the permeabilities, P, show a spatial variation that is clearly different from that of the cell sizes, L. For instance, the central low-permeability region is considerably larger than the region with large cell diameters, while in the periphery an increase of both, cell size and permeability, is observed. This indicates that both parameters are independent of each other. The central area of the carrot exhibits a very low permeability in both in-plane directions; this is consistent with the assumption that those cells are oriented longitudinally (out-of-plane) and have a high permeability only in longitudinal direction for water transport. Our results for P agree very well with data published by Sibgatullin et al. (2010, Fig. 9f) with in-plane permeabilities P' between about $1 \times 10^{-5}\,\mathrm{m/s}$ and $4 \times 10^{-5}\,\mathrm{m/s}$, which correspond to values of our $P = P'/D_0$ between about 0.007 and $0.03\,\mathrm{\mu m^{-1}}$. Unfortunately, the data by Sibgatullin et al. (2010) does not allow an in-plane anisotropy analysis, and we did not find any other reference values in the literature for anisotropy effects of the permeabilities.

The proposed method for the evaluation of $D_{\mathrm{meas}}(\tau)$ contains two steps: (1) the simulation of $\tilde{D}_{\mathrm{eff}}(\tilde{\tau};\tilde{P})$ for a large range of dimensionless parameters $\tilde{\tau}$ and $\tilde{P}$ and (2) the fitting of $D_{\mathrm{meas}}(\tau)$ to interpolated values of the simulation. Since D_0 corresponds to the extrapolated maximum of $D_{\mathrm{meas}}(\tau)$, P is related to the limit of $D_{\mathrm{meas}}(\tau)$ at long τ, and L is related to the initial slope of $D_{\mathrm{meas}}(\sqrt{\tau})$, these 3 parameters can be estimated uniquely from the measurement, if a sufficient number and range of diffusion times is included.

Ideally, $\tilde{D}_{\mathrm{eff}}(\tilde{\tau};\tilde{P})$ could be calculated directly for the required parameters during

least-squares fitting; however, even with current PC hardware, the numerical evaluation of (7) is too slow to be used for fitting – in particular, if pixelwise fitting for a large number of curves is required. A simplified evaluation technique is described in the Appendix, in which a small subset of sample points is given that enable a good approximation of the values of $\tilde{D}_{\text{eff}}(\tilde{\tau};\tilde{P})$. Using these sample points, the parameter fitting of measurements $D_{\text{meas}}(\tau)$ can be performed without the requirement of first simulating the large number of diffusion coefficients $\tilde{D}_{\text{eff}}(\tilde{\tau};\tilde{P})$.

In contrast to the approach by Sibgatullin et al. (2010), we did not apply any approximate renormalizations, but used a physical diffusion model to extract the parameters D_0, L, and P. Comparing the results of the pixelwise data analyses, we could obtain less noisy parameter maps than Sibgatullin et al. (2010) with clearly observable anisotropy properties at comparable spatial resolution.

The underlying model, i. e., diffusion between equidistant permeable membranes, is certainly a simplification of the actual properties of biological tissue. In particular, animal or human tissue typically consists of several compartments such as intracellular and extracellular spaces with different diffusion properties. Thus, the model proposed by Powles et al. (1992) can only be a first approximation to a more realistic description of water diffusion. Nevertheless, the quantitative results obtained in carrots are in good agreement with light microscopy indicating that – at least for plant tissue – the approximations are acceptable. Even for more complicated biological tissues, the model can be expected to approximate the actual diffusion behavior as long as the tissue is dominated by a single compartment with a typical structure size (e. g., a typical cell diameter), which is the case also for several kinds of animal tissue.

In conclusion, we demonstrated that the 4-parameter model $D(\tau;\ D_0, L, P)$ of diffusion between equidistant permeable membranes proposed by Powles et al. (1992) can be simplified to a dimensionless 2-parameter model $\tilde{D}(\tilde{\tau};\ \tilde{P})$ which can then be used for the quantitative determination of tissue parameters (D_0, L, P) based on diffusion MRI with multiple diffusion times. Measurements in a carrot showed a good agreement in particular of the cell diameter, L, determined by DWI and by light microscopy.

Appendix. Approximation of simulation results

We used the large number of simulated values $\tilde{D}_{\text{eff}}(\tilde{\tau};\tilde{P})$ (evaluated for $60 \times 35 = 2100$ combinations of parameters) to find an approximation which can be described by a much smaller amount of data. Therefore, we searched for a smaller grid of sample values that optimally approximates the original simulation results $\tilde{D}_{\text{eff}}(\tilde{\tau};\tilde{P})$. Interpolation between the grid points was performed with the GNU Octave two-dimensional interpolation routine `interp2` and the `pchip` (piece-wise cubic hermite interpolating polynomial) method.

A coarse $N \times N$ grid was defined with the same minimum and maximum values as the original simulation grid ($\tilde{\tau}_{\text{min}} = 0, ..., \tilde{\tau}_{\text{max}} = 225;\ \tilde{P}_{\text{min}} = 0, ..., \tilde{P}_{\text{max}} = 30$) and $(N-2) \times (N-2)$ grid points in between. The positions of these central points was

Table A1. Data evaluation with fully sampled (60×35) grid and 6×6 approximation

ROI	L (µm)			P (µm^{-1})			D_0 (µm^2/s)		
	full	6×6	Δ (%)	full	6×6	Δ (%)	full	6×6	Δ (%)
Radial in-plane orientation:									
1	72.6	72.8	+0.2	0.0072	0.0071	−0.4	1713	1711	−0.1
2	61.4	60.2	−1.9	0.0092	0.0096	+3.6	1658	1664	+0.3
3	24.5	24.6	+0.1	0.0160	0.0161	+0.6	1422	1417	−0.4
4	29.2	28.9	−0.7	0.0274	0.0277	+1.2	1531	1526	−0.4
5	32.4	32.4	−0.1	0.0258	0.0259	+0.4	1568	1561	−0.5
6	36.9	36.7	−0.6	0.0301	0.0302	+0.6	1625	1618	−0.4
Azimuthal in-plane orientation:									
1	76.2	75.9	−0.4	0.0067	0.0068	+1.3	1711	1712	+0.03
2	70.5	69.2	−1.8	0.0085	0.0088	+3.6	1661	1666	+0.3
3	21.3	21.4	+0.5	0.0135	0.0133	−1.4	1354	1348	−0.4
4	24.0	23.9	−0.4	0.0275	0.0281	+2.1	1514	1505	−0.6
5	38.5	37.4	−2.8	0.0307	0.0315	+2.5	1592	1593	+0.1
6	54.0	49.7	−7.9	0.0390	0.0427	+9.7	1656	1669	+0.7

varied and the values $\tilde{D}_{\text{eff}}(\tilde{\tau}; \tilde{P})$ at the new (coarse) grid were taken from the simulation results (linearly interpolated if necessary). Then, the coarse $N \times N$ grid itself was interpolated using the `pchip` method and this interpolation was compared with the original simulation result based on the sum of the squared differences of both data sets. This sum was minimized as a function of the position of the $(N-2) \times (N-2)$ central grid positions for $3 \leq N \leq 7$. The optimal grid for $N = 6$ was used to implement a fit function presented in figure A1.

A comparison of the ROI data evaluation (mean values over 4 corresponding ROIs from the 4 ROI sets) with both the full simulation of $\tilde{D}_{\text{eff}}(\tilde{\tau}; \tilde{P})$ (on a 60×35 grid) and the approximated values from a 6×6 grid is shown in table A1. The differences between both approaches are small with an average (absolute) deviation of 1.7 % for L, of 3.0 % for P, and of 0.4 % for D_0. All individual deviations are below 10 %. The corresponding mean absolute deviations for (L, P, D_0) at other grid sizes are (10.5 %, 44.4 %, 7.0 %) for $N = 3$, (7.2 %, 17.4 %, 2.4 %) for $N = 4$, (4.3 %, 8.9 %, 0.8 %) for $N = 5$, and (2.1 %, 3.2 %, 0.5 %) for $N = 7$; thus, increasing the coarse grid size above $N = 6$ does not further improve the approximation for the given data points.

```
function Deff = Deff_approx6(tau, params)

% return effective diffusion coefficient Deff(tau) for an infinite system
% of equidistant permeable membranes (cf. Powles JG et al. 1992);
% (based on a 6x6 grid approximation to numerical simulation results)
% Input:
% * diffusion time tau (vector, units: s)
% * system properties (given as "params" vector):
%   * params(1): unrestricted diffusion coefficient D0 (units: um^2/s)
%   * params(2): membrane distance L (units: um)
%   * params(3): membrane permeability P (units: 1/um)
% Output:
% * effective diffusion coefficient Deff (units: um^2/s)

D0 = params(1); L = params(2); P = params(3);

% transform to dimensionless (="_DL") parameters
P_DL     = L * P;
tau_DL   = 2*D0/L^2 * tau;
sigma_DL = sqrt(tau_DL);

% define coarse 6x6 grid approximating Deff_DL(tau_DL, P_DL)
P_DL_coarse     = [0.00000 0.34961 1.20024 3.44181 9.28077 30.00000];
sigma_DL_coarse = [0.00000 0.16626 0.68696 1.15545 2.35518 15.00000];
Deff_DL_coarse  = [
   5.0000e-01  5.0000e-01  5.0000e-01  5.0000e-01  5.0000e-01  5.0000e-01
   4.1177e-01  4.1601e-01  4.2561e-01  4.4317e-01  4.6517e-01  4.8567e-01
   1.5964e-01  2.2143e-01  3.0874e-01  3.9635e-01  4.5267e-01  4.8406e-01
   6.2298e-02  1.6439e-01  2.8715e-01  3.9140e-01  4.5180e-01  4.8397e-01
   1.5026e-02  1.4225e-01  2.8182e-01  3.9059e-01  4.5168e-01  4.8396e-01
   3.6994e-04  1.4867e-01  2.8658e-01  3.9189e-01  4.5193e-01  4.8399e-01 ];

% check constraints
P_DL = max(0, min(30, P_DL));
sigma_DL(sigma_DL > 15) = 15;

% calculate Deff
Deff_DL = interp2(P_DL_coarse, sigma_DL_coarse, Deff_DL_coarse,
                  P_DL, sigma_DL, 'pchip');
Deff = 2*D0 * Deff_DL;
```

Figure A1. Code (for GNU Octave) of approximated fitting function. The grid positions and the values of the 6×6 grid were determined numerically based on simulations on a much finer grid.

References

Fieremans E, Novikov D S, Jensen J H & Helpern J A 2010 Monte Carlo study of a two-compartment exchange model of diffusion *NMR Biomed.* **23**(7), 711–724.

Grebenkov D S 2007 NMR survey of reflected brownian motion *Rev. Mod. Phys.* **79**, 1077–1137.

Hahn E L 1950 Spin echoes *Phys. Rev.* **80**, 580–594.

Kim M H, Smith V P & Hong T K 1990 Evaluation of the function $\exp(x^2)\mathrm{erfc}(x)$ to higher precisions for higher order derivative polarography of CE-type electrode process *Bull. Korean Chem. Soc.* **11**(6), 497–505.

Knauss R, Schiller J, Fleischer G, Karger J & Arnold K 1999 Self-diffusion of water in cartilage and cartilage components as studied by pulsed field gradient NMR *Magn. Reson. Med.* **41**(2), 285–292.

Kunz N, Sizonenko S V, Hüppi P S, Gruetter R & van de Looij Y 2013 Investigation of field and diffusion time dependence of the diffusion-weighted signal at ultrahigh magnetic fields *NMR*

Biomed. **26**(10), 1251–1257.

Le Bihan D, Breton E, Lallemand D, Grenier P, Cabanis E & Laval-Jeantet M 1986 MR imaging of intravoxel incoherent motions: application to diffusion and perfusion in neurologic disorders *Radiology* **161**(2), 401–407.

Lether F G 1990 An elementary approximation for $\exp(x^2)\mathrm{erfc}(x)$ *J. Quant. Spectrosc. Radiat. Transfer* **43**(6), 511–513.

Mitra P P, Sen P N, Schwartz L M & Le Doussal P 1992 Diffusion propagator as a probe of the structure of porous media *Phys. Rev. Lett.* **68**(24), 3555–3558.

Pfeuffer J, Flögel U, Dreher W & Leibfritz D 1998 Restricted diffusion and exchange of intracellular water: theoretical modelling and diffusion time dependence of 1H NMR measurements on perfused glial cells *NMR Biomed.* **11**(1), 19–31.

Portnoy S, Flint J J, Blackband S J & Stanisz G J 2013 Oscillating and pulsed gradient diffusion magnetic resonance microscopy over an extended b-value range: implications for the characterization of tissue microstructure *Magn. Reson. Med.* **69**(4), 1131–1145.

Powles J G, Mallett M J D, Rickayzen G & Evans W A B 1992 Exact analytic solutions for diffusion impeded by an infinite array of partially permeable barriers *Proc. R. Soc. Lond. A* **436**, 391–403.

Pyatigorskaya N, Le Bihan D, Reynaud O & Ciobanu L 2013 Relationship between the diffusion time and the diffusion MRI signal observed at 17.2 Tesla in the healthy rat brain cortex *Magn. Reson. Med.* **DOI:10.1002/mrm.24921**, (epub ahead of print).

Russell G, Harkins K D, Secomb T W, Galons J P & Trouard T P 2012 A finite difference method with periodic boundary conditions for simulations of diffusion-weighted magnetic resonance experiments in tissue *Phys. Med. Biol.* **57**(4), N35–N46.

Sen P N 2004 Time-dependent diffusion coefficient as a probe of geometry *Concepts Magn. Reson. Part A* **23A**(1), 1–21.

Sibgatullin T A, Vergeldt F J, Gerkema E & Van As H 2010 Quantitative permeability imaging of plant tissues *Eur. Biophys. J.* **39**(4), 699–710.

Stejskal E O 1965 Use of spin echoes in a pulsed magnetic-field gradient to study anisotropic, restricted diffusion and flow *J. Chem. Phys.* **43**(10), 3597–3603.

Stejskal E O & Tanner J E 1965 Spin diffusion measurements: Spin echoes in the presence of a time-dependent field gradient *J. Chem. Phys.* **42**(1), 288–292.

Tanner J E 1978 Transient diffusion in a system partitioned by permeable barriers. application to NMR measurements with a pulsed field gradient *J. Chem. Phys.* **69**(4), 1748–1754.

Tanner J E & Stejskal E O 1968 Restricted self-diffusion of protons in colloidal systems by the pulsed-gradient, spin-echo method *J. Chem. Phys.* **49**(4), 1768–1777.

Taylor D G & Bushell M C 1985 The spatial mapping of translational diffusion coefficients by the NMR imaging technique *Phys. Med. Biol.* **30**(4), 345–349.

Van A T, Holdsworth S J & Bammer R 2014 In vivo investigation of restricted diffusion in the human brain with optimized oscillating diffusion gradient encoding *Magn. Reson. Med.* **71**(1), 83–94.

Wayne R C & Cotts R M 1966 Nuclear-magnetic-resonance study of self-diffusion in a bounded medium *Phys. Rev.* **151**, 264–272.

Weber T, Ziener C H, Kampf T, Herold V, Bauer W R & Jakob P M 2009 Measurement of apparent cell radii using a multiple wave vector diffusion experiment *Magn. Reson. Med.* **61**(4), 1001–1006.

Woessner D E 1963 N.M.R. spin-echo self-diffusion measurements on fluids undergoing restricted diffusion *J. Phys. Chem.* **67**(6), 1365–1367.

Xu J, Does M D & Gore J C 2007 Numerical study of water diffusion in biological tissues using an improved finite difference method *Phys. Med. Biol.* **52**(7), N111–N126.

Yablonskiy D A & Sukstanskii A L 2010 Theoretical models of the diffusion weighted MR signal *NMR Biomed.* **23**(7), 661–681.

Zhong J H & Gore J C 1991 Studies of restricted diffusion in heterogeneous media containing variations in susceptibility *Magn. Reson. Med.* **19**(2), 276–284.